NIH Public Access
Author Manuscript
J Am Chem Soc. Author manuscript; available in PMC 2011 December 29.

Published in final edited form as:
J Am Chem Soc. 2010 December 29; 132(51): 18292–18300. doi:10.1021/ja106820e.

Conformational remodeling of femtomolar inhibitor-acetylcholinesterase complexes in the crystalline state

Yves Bourne[1,*], **Zoran Radic**[2], **Palmer Taylor**[2], and **Pascale Marchot**[3,*]

[1]Architecture et Fonction des Macromolécules Biologiques (AFMB, CNRS UMR-6098), Universités d'Aix-Marseille, Campus Luminy - Case 932, F-13288 Marseille cedex 09, France. yves.bourne@afmb.univ-mrs.fr

[2]Department of Pharmacology, Skaggs School of Pharmacy and Pharmaceutical Sciences, University of California San Diego, La Jolla, CA 92093-0657, USA

[3]Centre de Recherche en Neurobiologie-Neurophysiologie de Marseille (CRN2M, CNRS UMR-6231), Institut Fédératif de Recherche Jean Roche, Faculté de Médecine Secteur Nord, Universités d'Aix-Marseille, CS80011, F-13344 Marseille cedex 15, France. pascale.marchot@univmed.fr

Abstract

The active center of acetylcholinesterase (AChE), a target site for competitive inhibitors, resides centrosymmetric to the subunit at the base of a deep, narrow gorge lined by aromatic residues. At the gorge entry, a peripheral site encompasses overlapping binding loci for non-competitive inhibitors, which alter substrate access to the gorge. The click-chemistry inhibitor TZ2PA6 links the active center ligand, tacrine, to the peripheral site ligand, propidium, through a biorthogonal reaction of an acetylene and an azide that forms either a *syn1* or an *anti1* triazole. Compared with wild-type mouse AChE, a Tyr337Ala mutant displays full catalytic activity, albeit with two to three orders of magnitude higher affinities for the TZ2PA6 *syn1* and *anti1* regioisomers, reflected in low femtomolar K_d values, diffusion-limited association and dissociation half-times greater than one month and one week, respectively. Three structures of each of the co-crystallized *syn1* and *anti1* complexes of the Tyr337Ala mutant were solved at three distinct times of crystal maturation, consistent with or exceeding the half-lives of the complexes in solution, while crystalline complexes obtained from soaked Tyr337Ala crystals led to picturing "freshly formed" complexes. The structures, at 2.55-2.75Å resolution, reveal a range of unprecedented conformations of the bound regioisomers, not observed in the wild-type AChE complexes, associated with concerted positional rearrangements of side chains in the enzyme gorge. Moreover, time-dependent conformational remodeling of the crystalline complexes appears to correlate with the dissociation half-times of the solution complexes. Hence for the tight-binding TZ2PA6 inhibitors, the initial complexes kinetically driven in solution slowly form more stable complexes governed by thermodynamic equilibrium and observable in mature crystals.

Keywords

Acetylcholinesterase; active site gorge; click chemistry; conformational change; crystal structure; femtomolar dissociation constant; peripheral site; triazole

[*]Corresponding authors, YB and PM.

Supporting Information Available: Supplementary Figure S1 and associated references. This material is available free of charge via the Internet at http://pubs.acs.org.

NIH-PA Author Manuscript
NIH-PA Author Manuscript
NIH-PA Author Manuscript

NIH-PA Author Manuscript

NIH-PA Author Manuscript

NIH-PA Author Manuscript

1. Introduction

Acetylcholinesterase (AChE) rapidly terminates cholinergic neurotransmission by catalyzing the hydrolysis of the neurotransmitter, acetylcholine, at peripheral and central synapses.[1] Inhibitors of AChE have been used for over a century in various therapeutic strategies in certain neuromuscular, ophthalmic, and cognitive disorders.[2] Competitive, reversible or irreversible inhibitors of AChE bind the active center, that contains the Glu/His/Ser catalytic triad and is located centrosymmetric to the molecule at the bottom of a deep and narrow gorge.[3] Non-competitive, reversible inhibitors and activators bind the peripheral anionic site (PAS), an allosteric surface site encompassing overlapping subsites located at the gorge entrance.[4] Some other inhibitors with an extended structure and harboring two functional binding moieties bind at both sites and occupy the gorge pathway.[5,6] Such ligands typically display higher affinities than those of the individual components and simultaneously inhibit ACh hydrolysis and impair PAS functionality.[7]

The 1,3-dipolar cycloaddition reaction between azides and terminal alkynes has become a potentially powerful approach for drug discovery.[8-11] When reactants are attached to a tetrahydroaminoacridine (tacrine) tricyclic moiety and a phenyl-phenanthridinium moiety (propidium), respectively selective for the active center and PAS of the enzyme, the biorthogonal reaction occurs at a considerable rate if conducted *in situ*, *i.e.* inside the active center gorge of AChE (Scheme 1).[11,12]

Moreover, from a series of reagent, building block combinations, the AChE surface preferentially catalyzes the formation of a *syn1*-triazole regioisomer with defined substitution positions and linker distances. Inhibition measurements revealed this isomer to be a very high affinity, reversible inhibitor of AChE, with association rate constants near the diffusion limit and a sub-picomolar equilibrium dissociation constant (K_d) reflected in the slow dissociation rates for mouse AChE (mAChE) (Table 1). The corresponding *anti1*-isomer, not formed by the enzyme but generated *in vitro*, proved to be a respectable though weaker inhibitor with “only” near-picomolar K_d value for mAChE. Triazole formation, midway down the gorge, required the two building blocks be positioned to accommodate the gorge geometry. This approach also permitted us to identify other motifs, phenyltetrahydroisoquinoline, as candidate peripheral site ligands.[13]

Comparative crystallographic analysis of the *syn1*- and *anti1*-mAChE complexes revealed distinctive orientations of the phenyl-phenanthridinium moieties associated with compensating conformational changes of Trp286 at the enzyme PAS.[14] Moreover, the position of the triazole, along with regioisomer preference, suggested that the phenol side chain of AChE Tyr337 protruding into the active center gorge is a critical determinant of specificity. This prompted us to investigate, by site-directed mutagenesis, the role of some of the conserved aromatic side chains that line the active center gorge and establish direct interactions with the bound *anti1* and *syn1* isomers, as observed in the structures.[14] Following mutagenesis of residue Trp286 at the gorge entrance[14], we selectively substituted the facing residues Tyr124 and Tyr337 in the constricted region in the gorge and residue Tyr72 in the gorge path, and characterized the mutants through kinetic binding assays. Compared to mAChE, mutant Tyr337Ala was found to display two to three orders of magnitude greater affinities for the TZ2PA6 *anti1* and *syn1* isomers, leading to K_d values in the low femtomolar range (Table 1).

To explore the structural basis for such further increases in otherwise very high affinities, we solved crystal structures of the Tyr337Ala mutant and of its co-crystallized complexes with the two TZ2PA6 isomers. However, instead of solving a single structure from a lone crystal for each complex as is usually done, from crystals of a same “litter” we collected distinctive

NIH-PA Author Manuscript

NIH-PA Author Manuscript

NIH-PA Author Manuscript

data sets at increasing crystal maturation times corresponding to shorter than, equal to and longer than the half-time for complex dissociation in solution ($t_{1/2}$). Structural analysis of the co-crystallized Tyr337Ala complexes and their comparison with the previously solved mAChE complexes provide evidence for a range of torsional/rotational (*anti1*) and compressive/extensive (*syn1*) rearrangements of the bound regioisomers associated with compensatory reorientations of side chains within the enzyme gorge, while the time course of conformational remodeling of the complexes in the crystals appears to correlate with the dissociation half-times in solution. Analysis of crystalline *anti1* and *syn1* complexes obtained from soaked Tyr337Ala crystals led to picturing "freshly formed" complexes. Finally, analysis of a Tyr337Ala crystal soaked with mixed *anti1* and *syn1* regioisomers led to a predominant *syn1* complex, demonstrating preferential trapping of the slowest dissociating ligand present in a mixture of related compounds. Hence for the tight-binding TZ2PA6 inhibitors, the initial complex formed in solution and observable from a soaked crystal, continues to evolve in maturing co-crystals to achieve lower energy states and better fit.

2. Experimental methods

2.1. Preparation and crystallization of the complexes and data collection

The mAChE mutant Tyr337Ala, generated by site-directed mutagenesis and expressed as a soluble protein in HEK-293 cells,[15] was purified by affinity chromatography using decamethonium desorption and dialyzed and prepared as previously described for mAChE[16]. This mutant displays catalytic parameters for ATCh (k_{cat}, K_m) similar to values for mAChE.[15] The specific activity of a concentrated, sterile-filtered solution was virtually unaltered after one year storage on ice.

The TZ2PA6 *anti1* and *syn1* isomers, synthesized and purified as tosylate salts as described, [11] were kind gifts from K.B. Sharpless and H.C. Kolb (Dept of Chemistry and Skaggs Institute for Chemical Biology, The Scripps Research Institute, La Jolla, CA). Titration of the isomer stock solutions was carried out spectrophotometrically ($\varepsilon_{490\ nm} = 6000\ M^{-1}cm^{-1}$). [17] The complexes for cocrystallization were prepared using Tyr337Ala at ca. 5 mg/ml and a 2-fold molar excess of each inhibitor (overnight equilibration, 4°C). The unbound ligand was removed and the complexes concentrated to ca. 10 mg/ml using ultrafiltration with controlled rincing. Total inhibition of activity of the complexes was assessed spectrophotometrically[18] using enzyme concentrations well above the K_d's.

The Tyr337Ala mutant and its preformed *anti1* and *syn1* complexes were crystallized at 4°C by vapor diffusion using hanging drops (1 μl) and a protein-to-well solution ratio of 1:1 with PEG-600 25-35% (v/v) in 50-100 mM Hepes, pH 6.0-7.0, or with PEG-550 MME 30% (v/v) in 50 mM Na acetate, pH 7.5, as the reservoir solution. The crystals appeared rapidly, grew to a suitable size within a week and showed limited enlargement thereafter. For each of the co-crystallized complexes, three data sets were collected from crystals that appeared at the same time in the same drop (defined as the same "litter" of crystals) but were flash-cooled at distinct maturation times roughly corresponding to one week, one month and ten months (referred to as "1-wk", "1-mth" and "10-mth" data sets and structures, respectively). For the co-crystallized *syn1* complex, two additional data sets diffracting to *ca*. 3.0 Å resolution were collected after 18 months (i.e., $15 \times t^{1/2}$) and 3 years ($30 \times t_{1/2}$) of crystal maturation, leading to similar *syn1* conformations as observed in the 10-mth structure (data not shown).

Formation of *anti1* and *syn1* complexes by soaking Tyr337Ala crystals was carried out at 4°C in 20 μl sitting drops made of the well solution supplemented with 50 μM of *anti1*, *syn1*, or both for 24-36 hours. Soaks longer than two days led to ill-diffracting crystals. All crystals were directly flash-cooled in the nitrogen gas stream (100°K). They all belonged to

NIH-PA Author Manuscript

NIH-PA Author Manuscript

NIH-PA Author Manuscript

the orthorhombic space group $P2_12_12_1$ with unit cell dimensions a = 79.7 Å, b = 111.9 Å, c = 226.5 Å. Oscillation images were integrated with DENZO[19] and data scaled and merged with SCALA[20] (Table 2).

2.2. Structure determination and refinement

The apo mAChE structure (accession code, 1J06)[17] without solvent was used as a starting model to refine the structures of the Tyr337Ala mutant and each of its *anti1* and *syn1* complexes with the program REFMAC[21] (Table 2). Rigid-body refinement was performed on each of the two subunits in the crystalline dimer using all data followed by cycles of restrained refinements. A random set of reflections (2%, 2255 reflections) taken from the mAChE-SCh complex structure (2HA2)[22] was set aside for cross validation purposes In each case, the resulting sigmaA-weighted 2Fo-Fc and Fo-Fc electron density maps were used to position the inhibitor and correct the protein model with the graphics program COOT[23].

The final structures, comprising one Tyr337Ala mutant and its eight co-crystallized and three soaked complexes, comprise residues Glu1-Ala541 and Glu4-Thr540 for the two respective enzyme molecules in the asymmetric unit[17]. High temperature factors and weak electron densities are associated with the short Ω loop Cys257-Cys272 and the surface loop region Asp491-Pro498. In the Tyr337Ala structure, traces of decamethonium and acetate arising from the purification and crystallization procedures, respectively, are detected in the active site gorge of one subunit in the dimer, as found in previous mAChE structures (accession codes, 1MAA and 1N5R). The stereochemistries of the structures were analyzed with MolProbity[24]; with the exception of the catalytic Ser203, no residues were found in the disallowed regions of the Ramachandran plot. The rmsd's between the structures of apo mAChE, Tyr337Ala, the *anti1*- and *syn1*-mAChE complexes, and each of the *anti1*- and *syn1*-Tyr337Ala complexes are in the 0.15-0.32 Å range for 534 Cα atoms. The atomic coordinates and structure factors of the Tyr337Ala structure, the six 1-wk, 1-mth and 10-mth structures of co-crystallized *anti1* and *syn1* complexes and the three structures of *anti1* and *syn1* complexes obtained from soaked crystals have been deposited with the Protein Data Bank (cf. Table 2 for accession codes). Figures were generated with PyMOL[25].

2.3. Inhibition / binding studies

The Tyr124Gln and Tyr72Asn/Tyr124Gln/Trp286Ala mutants of mAChE were expressed, sequence verified and concentrated from the expression medium as described.[15,22] Kinetic analysis of *anti1* and *syn1* binding to these along with the Tyr337Ala mutants used conventional procedures. The association (k_{on}) and first-order dissociation rate constants (k_{off}) and the equilibrium dissociation constants (K_d) of the *anti1* and *syn1* isomers for Tyr337Ala were determined as described.[11,14] Briefly, association rates were determined by direct stopped-flow measurements of AChE tryptophan quenching upon inhibitor binding, while dissociation rates were determined by spectrophotometric measurements of the time-dependant recovery of AChE activity[18] of the AChE-inhibitor complex diluted 5000-fold into a 250 μg/ml solution of herring sperm DNA (Boehringer) or a 50-400 nM solution of the inactive mAChE mutants Ser203Ala[22] or Ser203Ala/Tyr337Ala, or a mixture of both DNA and Ser203Ala mutant. Both DNA and mAChE mutants were used as a scavenger to sequester the released inhibitor through its phenanthridinium moiety (DNA) or overall structure (mAChE mutants). All measurements were performed in 0.1 M $NaPO_4$, pH 7.0, at 22°C.

NIH-PA Author Manuscript

NIH-PA Author Manuscript

NIH-PA Author Manuscript

3. Results and discussion

The mAChE mutants Tyr124Gln, Trp286Ala, Tyr337Ala and Tyr72Asn/Tyr124Gln/Trp286Ala were designed previously to mimic tertiary structure of BChE in the PAS domain of mAChE along with, for Tyr337Ala, the choline binding site.[15] Mutant Trp286Ala was analyzed for *anti1* and *syn1* binding in a previous study[14] while the other three mutants were analyzed for *anti1* and *syn1* binding in the present study (Table 1).

3.1. Kinetic analysis of TZ2PA6 isomer binding to the mAChE mutants

Kinetic parameters recorded in solution for *anti1* and *syn1* binding to the Tyr124Gln mutant led to similar association rates, and hence, comparable dissociation constants as for mAChE (Table 1). For the Trp286Ala and triple mutants, 5-fold to 340-fold greater dissociation constants dictated by up to 30-fold slower association and 10-fold slower dissociation were recorded, consistent with involvement of these residues that line the active site gorge in stabilization of either of the *anti*- and *syn*-triazoles in mAChE. For the mutants, particularly the triple mutant, conformationally distinct complexes in the gorge confines can thus be expected from removal of large aromatic side chains.

In contrast, for the Tyr337Ala mutant compared to mAChE, similar association rates but much lower dissociation rates, by 3000-fold for the *anti1* and 550-fold for the *syn1*, were recorded, whereas they were lowered by only 350-fold and 85-fold when compared with *T. californica* AChE, with its Phe substitution for Tyr337 (Table 1). The resulting femtomolar affinities largely reflect greater activation barriers, and place the TZPA isomers at a similar free energy of binding as that of 1,1,1-trifluoroacetophenone derivatives towards AChE or biotin towards streptavidin, despite a higher number of non-hydrogen atoms (Supporting Information, Fig. S1).[26] Compared with the *anti1* isomer, the 4-fold greater affinity of the *syn1* isomer for the Tyr337Ala mutant also arises from a 5-fold lower dissociation rate. This results in half-lives in solution of more than one month ($t_{1/2}$: 37 days) for the *syn1* complex and one week ($t_{1/2}$: 7.3 days) for the *anti1* complex, compared with $t_{1/2}$ values of 98 min and 3 min for the respective mAChE complexes. This also suggests that in the crystallization set-up, where dissociation is largely precluded by the high protein concentration of the complexes (10^7-10^9-fold the K_d in the mother liquor, presumably ≥ 10^{12}-fold the K_d in the crystal), equilibrium would be largely displaced toward complex formation, resulting in even higher stability of the complexes.

To explore this issue, for each of the co-crystallized *anti1*- and *syn1*-Tyr337Ala complexes we collected complementary data sets at increasing times of crystal maturation corresponding to smaller, near or greater the half-time values for complex dissociation in solution (Table 2). Another set of complexes, obtained by soaking Tyr337Ala crystals with individual or mixed inhibitors for times much shorter than the solution half-lives of the respective complexes (cf. Section 2.1.), was also analyzed (Table 2).

3.2. Overall fold of the Tyr337Ala mutant

The structure of the Tyr337Ala mutant is identical to that of mAChE (rmsd 0.28 Å for 535 Ca atoms), except at the substitution position where replacement of the bulky Tyr phenol ring by the small Ala methyl group enlarges, by ~2.5 Å, the gorge internal diameter (Fig. 1). Yet at this position the deviation for the gorge walls is only ~0.5 Å, indicating that the gorge shape is virtually unaltered and supporting catalytic activity similar to mAChE (data not shown). For each of the *anti1*- and *syn1*-Tyr337Ala complexes, 1-wk, 1-mth and 10-mth structures were solved (Table 2). In all six structures, the bound inhibitors are well-ordered and their binding site may be deconstructed into the same three discrete loci as found for the *anti1*- and *syn1*-mAChE complexes: i) the active center at the base of the gorge where the

NIH-PA Author Manuscript

NIH-PA Author Manuscript

NIH-PA Author Manuscript

tacrine moiety binds; ii) an intervening site in the constricted region within the gorge that associates with the triazole moiety and adjacent methylene groups; iii) the PAS at the gorge rim where the phenylphenanthridinium moiety binds (Fig. 1).[14] However, significant differences in the conformations of the inhibitor molecules and the positions of side chains within the gorge are observed between each pair (*anti1* versus *syn1*) of the TZ2PA6-Tyr337Ala complexes.

3.3. The three *anti1*-Tyr337Ala complexes obtained by co-crystallization

The binding of the *anti1* isomer to Tyr337Ala in the 1-wk structure (corresponding to 1-fold the $t_{1/2}$ for *anti1*) drastically differs from its binding to mAChE (Figs. 2 and 3). At the bottom of the gorge, the tacrine moiety, although positioned similarly as in mAChE, is flipped upside-down and tilted, by ~25°, compared to its position in the *anti1*- and *syn1*-mAChE complexes. As a result, the polar interaction that, in the *anti1*- and *syn1*-mAChE complexes, occurs between the basal tacrine N8 atom and the backbone carbonyl of His447, is now swapped to involve the opposite N7 atom at the basis of the dimethylene linker connecting the tacrine and triazole.

At the region of constriction formed by the side chains of Tyr124, Phe297 and Phe338 some 5-8 Å into the gorge, where the substituting Ala337 side chain is located, the hooked conformation of the dimethylene chain dictates a distinct positioning for the triazole, which in the Tyr337Ala mutant is displaced by 3 Å laterally into the gorge and oriented ~90° away from its position in mAChE, as to mimic the tip of the missing Tyr337 phenol ring (Figs. 2 and 3). As a result, the triazole establishes stacking interactions in near-sandwich conformation between the central 6-heterocycle ring of tacrine and the Phe338 phenyl rings. In turn, the first methylene of the hexamethylene linker that connects the triazole and phenylphenanthridinium is positioned 2.3 Å deeper into the gorge and adopts an extended, linear conformation instead of the curved shape observed in the *anti1*-mAChE complex. The large differences in the triazole and hexamethylene positions in the Tyr337Ala mutant compared to mAChE are associated with discrete positional rearrangement of the Tyr124 and Tyr341 side chains that line the gorge wall.

At the PAS, the phenanthridinium intercalates between the Tyr72 and Trp286 side chains while the Trp286 side chain, dislodged from the PAS surface, adopts a solvent-exposed position similar to its position in the *syn1*-mAChE complex (Fig. 2). However, compared to this complex, a ~180° flip of the Trp286 side chain now induces a different, albeit still parallel, stacking interaction with the phenanthridinium. In fact, the intercalated phenanthridinium stabilizes an alternate minor conformation of the Trp286 side chain, flipped by 150°, reminiscent of that observed for the corresponding Trp279 residue in the TcAChE-NF595 complex[27]. The mode of binding of the phenanthridinium ring at the PAS, that drastically differs from that observed in the *anti1*-mAChE complex, results in a deeper positioning of the triazole into the gorge associated with an extended conformation of the hexamethylene linker.

Analysis of the *anti1*-Tyr337Ala complex in the 1-mth structure (4-fold the $t_{1/2}$) compared to the 1-wk structure reveals no significant differences in the isomer and enzyme conformations at the bottom of the gorge and the mid-gorge region of constriction (Fig. 2). Yet at the PAS, the Trp286 side chain, dislodged from the PAS surface, is positioned mid-way the two alternate positions seen in the 1-wk structure with no significant difference in the orientation of the phenanthridinium.

In the *anti1*-Tyr337Ala complex in the 10-mth structure (42-fold the $t_{1/2}$), the isomer and enzyme conformations are similar as in the 1-mth structure, whereas the Trp286 side chain adopts a similar conformation as the minor alternate conformation observed in the 1-wk

NIH-PA Author Manuscript

NIH-PA Author Manuscript

NIH-PA Author Manuscript

structure (Fig. 2). Hence even in the crystalline enzyme, the Trp286 side chain retains sufficient flexibility upon binding of a extremely potent ligand to undergo multiple fluctuating orientations, here exemplified by a 50° shutter-like movement of its indole ring in the 1-wk and 10-mth structures.

3.4. The three *syn1*-Tyr337Ala complexes obtained by co-crystallization

The binding of the *syn1* isomer to the Tyr337Ala mutant in the 1-wk structure (0.2-fold the $t_{1/2}$ for *syn1*) also differs from its binding to mAChE, besides a similarly oriented tacrine at the base of the gorge (Figs. 2 and 3). At the region of constriction, the triazole is shifted (by 1 Å) deeper into the gorge where it undergoes a near-parallel stacking interaction with the tacrine central amino-substituted ring. In turn, the hexamethylene linker is also shifted down (by ~1.5 Å) into the gorge, a feature that resembles the differences seen in the positions of the linker between the *anti1* and *syn1* isomers bound to mAChE[14].

At the PAS, the slightly deeper position of the triazole causes the *syn1* phenylphenanthridinium to adopt yet another distinct conformation, not observed in either structures of the *anti1*-Tyr337Ala or *anti1*- and *syn1*-mAChE complexes (Figs. 2 and 3). The phenanthridinium, here oriented perpendicular to the gorge axis with one face buried some 2 Å deep into the gorge and the other face exposed to the solvent, totally occludes the gorge entry. One of the distal ring is anchored to the Leu289-Arg296 loop region, with the nitrogen hydrogen bonded to the Ser293 and Arg296 carbonyl atoms, while the opposite distal ring weakly establishes an edge-to-face interaction with the Tyr341 phenol ring. The exocyclic phenyl ring in the phenanthridium inserts between the Tyr341 and Trp286 side chains, while the Trp286 side chain, in the typical orientation of apo mAChE, establishes van der Waals interactions with the phenyl ring. The newly positioned phenylphenanthridinium induces a ~40° arc motion of the Tyr72 phenol ring and a 30° tilt of the Tyr341 phenyl ring, respectively located on each side of the gorge entrance compared to their respective positions in the *syn1*-mAChE structure. In fact, the final density maps reveal additional electron density in the vicinity of the phenyl ring that could correspond to an alternate, minor abundance conformation of the *syn1* phenanthridinium, not observed in the other *anti1*- or *syn1*-Tyr337Ala complex structures.

Analysis of the *syn1*-Tyr337Ala complex in the 1-mth structure (0.8-fold the $t_{1/2}$) reveals, for the bound tacrine and triazole at the base of the gorge and the hexamethylene linker at the region of constriction, similar positions and orientations as in the 1-wk structure (Fig. 2). At the PAS however, the phenanthridinium ring is oriented ~115° away from its position in the 1-wk structure as to match the orientation previously observed in the *syn1*-mAChE complex (Fig. 3). Consequently, the Trp286 side chain is dislodged from the PAS surface and swings towards the solvent to adopt a conformation that will be retained in the 10-mth structure (8-fold the $t_{1/2}$) (Fig. 2). Hence, in two distinctively matured crystals grown from the same *syn1*-Tyr337A complex, two distinct conformations of the phenanthridinium ring were trapped at the PAS. Moreover, the ligand pose and enzyme conformation observed in the 10-mth structure are essentially retained in even older complexes (cf. Section 2.1.), consistent with a thermodynamic equilibrium being attained at maturation times matching the solution half-lives.

These comparative data, combined with the structures of mAChE bound with the same inhibitors, demonstrate that albeit a femtomolar affinity, distinct conformations of the inhibitor coupled to conformational adaptations at the PAS exist, some of minor abundance, and thus reflect the behavior of the enzyme in solution. This is well exemplified by the presence of two alternate conformations of the Trp286 side chain in the *syn1*-Tyr337Ala complex in the 10-mth structure, of which one is similar to that in the 1-mth structure (Fig. 2).

NIH-PA Author Manuscript

NIH-PA Author Manuscript

NIH-PA Author Manuscript

3.5. The *anti1*- and *syn1*-Tyr337Ala complexes obtained by crystal soaking

Compared with the *anti1*-Tyr337Ala structures obtained by co-crystallization, that obtained from a crystal soaked for a time 7-fold shorter than the complex half-life (Table 2; cf. Section 2.1.) shows a similar mode of binding for the *anti1* isomer as found in the 1-wk structure, with only slight variations in the hexamethylene linker conformation and the Trp286 side chain orientation at the PAS (Fig. 2). In contrast, compared with the *syn1*-Tyr337Ala structures obtained by co-crystallization, that obtained from a soaked crystal (here for a time 30-fold shorter than the complex half-life (Table 2)) reveals two alternate conformations of the phenanthridinium ring at the PAS, of which each matches the orientation respectively identified in the *syn1*-Tyr337Ala 1-wk and 1-mth structures (Fig. 3). Hence, crystal soaking procedures led to picturing freshly formed complexes resembling more the complexes observed at crystal maturation times shorter than the solution half-lives.

In turn, the structure derived from soaking an equimolar *anti1*/*syn1* mixture reveals that the *syn1* isomer was predominantly trapped in the active site gorge, the *anti1* isomer being present in lower abundance only (Fig. 2). This is consistent with the kinetic data showing the higher affinity of the *syn1* isomer to reflect at least a 10-fold lower dissociation rate. Hence, either isomer can occupy the active site gorge at the same rate, but the *syn1* complex, owing to its slower dissociation rate, prevents *anti1* from binding again. Moreover, in this complex the bound *syn1* adopts the most energetically favorable conformation observed in the mature *syn1*-Tyr337Ala 1-mth and 10-mth structures. Hence, “dynamic combinatorial X-ray crystallography” (or DCX) on a limited scale can be used to select, from a mixture of structurally related high-affinity inhibitors, the slowest dissociating one. This observation, along with the reported binding selectivity of crystalline TcAChE for the soaked *(R)- versus (S)*-enantiomers, with otherwise similar affinities, of bifunctional inhibitors E220[28] and tacrine-(10)-hypyridone[29], argues for a structure-based approach to conduct inhibitor discovery and optimization.

3.6. Implications of structure variation

Comparison of the structures obtained for complexes of mAChE and its Tyr337Ala mutant with the TZ2PA6 *anti1* and *syn1* regioisomers emphasizes the key role of the triazole located midway the gorge in dictating the orientation of the phenanthridinium at the PAS. This is consistent with our previous proposal that the 1.5 Å positional shift between the *anti1* and *syn1* triazoles within the mAChE gorge influences the orientation of the phenanthridinium ring. Here we show that in the absence of the protruding Tyr337 side chain, the *anti1* triazole adopts a deeper position within the gorge of the mutant, roughly equivalent to that observed for the *syn1* isomer bound to mAChE and resulting in a similar orientation of the intercalated phenanthridinium ring. Similarly, the deeper positioning of the *syn1* triazole in the Tyr337Ala mutant compared to its position in mAChE results in a new orientation of the phenanthridinium ring, which seems to be fluctuating between two distinct orientations as exemplified in the 1-wk and 1-mth structures (Fig. 2).

The Tyr337Ala mutant is the only one of our screened mutants where the affinities of both the *syn1* and *anti1* complexes *increase* rather than *decrease* over the wild-type enzyme, a feature that suggests that the presence of the aromatic ring places some steric constraints around the triazole. Indeed, mutation of the facing Tyr124 only moderately affects the binding affinitiy of the two inhibitors, consistent with the structures of the complexes (Table 1). Since the ligands bind at near the diffusion rate limitation, the enhanced affinity is reflected in a slower dissociation rate.

A comparison of the multiple structures points to the large differences in the overall conformation of the inhibitor bound to the mutant. Importantly, these conformations are not

NIH-PA Author Manuscript

NIH-PA Author Manuscript

NIH-PA Author Manuscript

specific to the crystalline phase, but rather could reflect the fact that reactants, when simultaneously bound, induce these minor abundance conformational changes. Indeed, a combination of flexibility of reactant chain length and subtle rearrangements of the key interacting side chains are required for the 1,3-dipolar cycloaddition reaction to occur. Therefore the conformational fluctuations seen in the trapped inhibitor could reflect the conformational behavior of reactants. Decay of fluorescence anisotropy experiments along with an overlay of all available mAChE crystal structures in complex with ligands or conjugates argue towards this point (Z. Radic, unpublished data).

However, what remains obscure is whether the freeze frame inhibitor *syn1*, initially tailored in the AChE active site gorge and formed *in situ*[11], comes from a minor abundance complex of the reactants and its formation is driven by proximity of the reactive azide or alkyne, or if reactant binding itself selects a dominant conformation. Our data highlight the dynamic behavior of the AChE gorge, most particularly near its rim, and are consistent with the concept of protein breathing motions that are altered by the reactants. In the crystal, local packing forces do not modify the thermodynamic energy balance, selecting different conformations. Indeed, whereas the rigid *anti1* isomer adopts an elongated conformation within the gorge and has to fold into a hook in the catalytic pocket and rotate its top and bottom moieties in opposite directions (like a classic pepper mill) to become shorter, the highly flexible *syn1* isomer adopts a compacted and torturous conformation that can easily be compressed or extended (like a spring), depending on the position of the triazole into the gorge that influences the orientation of the phenantridinium at the PAS. The modes of interaction between the isomers and the Tyr337Ala mutant of mAChE, dominated by apolar interactions with contribution of conserved bridging water molecules, are similar for each of the six co-crystallized complexes, indicating that the overall shape rather than a particular mode of interaction might be a predominant factor for this gain in affinity. At the PAS, the intercalation of the phenylphenanthridinium between the Trp286 and Tyr72 side chains, so far only seen for the *syn1* isomer bound to mAChE[14] and now extended to the *anti1* isomer bound to Tyr337Ala, could significantly contributes to the large gain in affinity. Indeed, this peculiar conformation at the PAS could favor a near parallel rather than an antiparallel orientation of the azide and alkyne reactants (*syn1*- over *anti1*), causing the bond distance between the tacrine and phenanthridium moieties to be foreshortened by ~1.2 - 1.4 Å.

4. Conclusions

The conformational and positional differences observed throughout the four structures of the *anti1*-Tyr337Ala complex on one hand and four structures of the *syn1*-Tyr337Ala complex on the other hand (one soaked and three co-crystallized complexes in each case) appear to follow the increasing ratio of maturation time to dissociation half-time and hence, the time required for optimal stabilization of the respective crystalline complexes. These differences are particularly critical for the phenylphenanthridinium/hexamethylene portion of the inhibitors and surrounding enzyme residues in the upper part of the gorge and at the PAS, whereas the triazole/dimethylene/tacrine portion and surrounding residues at the bottom of the gorge adopt a definitive conformation and position perhaps as soon as each complex forms. These observations are consistent with the requirement for a more rigid active center to insure substrate specificity and rapid hydrolysis, while a more flexible PAS and gorge rim offer a wide range of recognition and binding capacities for allosteric regulation of catalysis.

The high affinities of the *syn1*- and *anti1*-Tyr337Ala complexes, with their dissociation times exceeding those of nucleation and crystal growth, afford a unique opportunity to examine conformational states dictated by ligand association, a kinetically dominated process, and those that reflect attainment of thermodynamic equilibrium, achieved by slow isomerization of the complex and/or multiple association and dissociation steps leading to

NIH-PA Author Manuscript

NIH-PA Author Manuscript

NIH-PA Author Manuscript

the slowest dissociating ligand becoming the dominantly bound one. A critical question is the conversion from the kinetically driven ligand poses to those found at longer times of equilibrium. Free ligand concentrations are high in the soaking experiments, but they are extremely low when co-crystals are formed at a stoichiometry of one ligand per active site. Hence, for the co-crystals one can exclude unbound ligand in the bulk solvent participating in the conversion in conformational states. This leaves two possibilities: (i) the conversion occurs *in situ* in the crystal analogous to a unimolecular isomerization; (ii) dissociation occurs into the limited space of the crystal solvent channels and then reassociation ensues, allowing the more slowly dissociating complexes to become dominant upon time. Since an isomerization of the complex and the dissociation process would both require Boltzman energy, they may be kinetically indistinguishable without assessing the presence of free ligand in the system. However, the very high protein concentrations in the crystal and surrounding solution (cf. Section 3.1.) along with the low temperature used for crystal formation and maturation (cf. Section 2.1.) most likely preclude complex dissociation. This suggests *in cristallo* isomerization to be the main conversion process from the kinetically driven complexes observed from the younger crystals to the thermodynamically driven equilibrium observed from the older crystals.

Distinctive large- or small-scale conformational changes of part or all of a crystalline receptor or enzyme have been evidenced by comparing structures solved from distinct crystal forms, crystallization conditions, complexes or any combination of these.[14,30-34] Alternative conformations of subunits within a same oligomeric protein have been reported,[34,35] and alternative conformations or binding positions of a bound ligand relative to its binding site have been described or predicted.[17,36,37] Yet, to our knowledge our study is a first to report a range of alternative conformations for both the ligand and protein in “same litter” crystalline complexes equilibrated over time periods consistent with or greater than their half-lives. Since kinetic and thermodynamic rules governing complex remodeling can still occur in the crystalline state, and since multiple poses of bound ligands of near equivalent free energy can be found in the structures, our data also suggest that statement “*the* crystal structure” of a ligand-protein complex should be interpreted as “*a* crystal structure” (i.e., perhaps amongst several possible) of this complex.

Supplementary Material

Refer to Web version on PubMed Central for supplementary material.

Acknowledgments

We are grateful to M. Juin and S. Conrod (CRN2M, Marseille) for assistance in crystallization and crystal soaking; to G. Sulzenbacher, S. Spinelli and M. Czjzek, (AFMB, Marseille) and the ID14 and ID29 staff of the European Synchrotron Radiation Facility (ESRF, Grenoble) for expert contribution to data collection; and to K.B. Sharpless and H.C. Kolb (Dept of Chemistry and Skaggs Institute for Chemical Biology, The Scripps Research Institute, La Jolla, CA) for the kind gift of the TZ2PA6 regioisomers, critical reading of the manuscript and fruitful discussions. This work was supported by grants from the USPHS and DAMD (to PT) and the Association Française contre les Myopathies and the CNRS-Direction des Relations Internationales (to PM).

Abbreviations

AChE	acetylcholinesterase (mAChE, recombinant from mouse)
PAS	peripheral anionic site
***syn1*-TZ2PA6**	3,8-diamino-6-phenyl-5-[6-[1-[2-[(1,2,3,4-tetrahydro-9-acridinyl)amino]ethyl]-1H-1,2,3-triazol-5_{syn}-yl]hexyl]-phenanthridinium ($C_{42}H_{45}N_8$)

NIH-PA Author Manuscript

NIH-PA Author Manuscript

NIH-PA Author Manuscript

***anti1*-TZ2PA6** 3,8-diamino-6-phenyl-5-[6-[1-[2-[(1,2,3,4-tetrahydro-9-acridinyl)amino]ethyl]-1H-1,2,3-triazol-4_{anti}-yl]hexyl]-phenanthridinium ($C_{42}H_{45}N_8$)

References

1. Quinn DM. Chem. Rev. 1987; 87:955–79.
2. Taylor P. Neurology. 1998; 51:S30–35. discussion S65-67. Review. [PubMed: 9674760]
3. Sussman JL, Harel M, Frolow F, Oefner C, Goldman A, Toker L, Silman I. Science. 1991; 253:872–9. [PubMed: 1678899]
4. Taylor P, Lappi S. Biochemistry. 1975; 14:1989–97. [PubMed: 1125207]
5. Greenblatt HM, Guillou C, Guénard D, Argaman A, Botti S, Badet B, Thal C, Silman I, Sussman JL. J. Am. Chem. Soc. 2004; 126:15405–11. [PubMed: 15563167]
6. Berman HA, Decker MM, Nowak MW, Leonard KJ, McCauley M, Baker WM, Taylor P. Mol. Pharmacol. 1987; 31:610–6. [PubMed: 3600605]
7. Haviv H, Wong DM, Silman I, Sussman JL. Curr. Top. Med. Chem. 2007; 7:375–387. [PubMed: 17305579]
8. Kolb HC, Sharpless KB. Drug Discov Today. 2003; 8:1128–37. [PubMed: 14678739]
9. Tron GC, Pirali T, Billington RA, Canonico PL, Sorba G, Genazzani AA. Med. Res. Rev. 2008; 28:278–308. [PubMed: 17763363]
10. Moorhouse AD, Haider S, Gunaratnam M, Munnur D, Neidle S, Moses JE. Mol. Biosyst. 2008; 4:629–42. [PubMed: 18493662]
11. Lewis WG, Green LG, Grynszpan F, Radic Z, Carlier PR, Taylor P, Finn MG, Sharpless KB. Angew Chem. Int. Ed. 2002; 41:1053–7.
12. Manetsch R, Krasinski A, Radic Z, Raushel J, Taylor P, Sharpless KB, Kolb HC. J. Am. Chem. Soc. 2004; 126:12809–18. [PubMed: 15469276]
13. Krasinski A, Radic Z, Manetsch R, Raushel J, Taylor P, Sharpless KB, Kolb HC. J. Am. Chem. Soc. 2005; 127:6686–92. [PubMed: 15869290]
14. Bourne Y, Kolb HC, Radic Z, Sharpless KB, Taylor P, Marchot P. Proc. Nat. Acad. Sci. USA. 2004; 101:1449–54. [PubMed: 14757816]
15. Radic Z, Pickering NA, Vellom DC, Camp S, Taylor P. Biochemistry. 1993; 32:12074–84. [PubMed: 8218285]
16. Marchot P, Ravelli RBG, Raves ML, Bourne Y, Vellom DC, Kanter J, Camp S, Sussman JL, Taylor P. Protein Sci. 1996; 5:672–9. [PubMed: 8845756]
17. Bourne Y, Taylor P, Radic Z, Marchot P. EMBO J. 2003; 22:1–12. [PubMed: 12505979]
18. Ellman GL, Courtney KD, Andres V Jr. Featherstone RM. Biochem. Pharmacol. 1961; 7:88–95. [PubMed: 13726518]
19. Otwinowski Z, Minor W. Methods Enzymol. 1997; 276:307–26.
20. CCP4, Collaborative Computational Project Number 4. Acta Crystallogr. 1994; D50:760–3.
21. Murshudov GN, Vagin AA, Dodson EJ. Acta Crystallogr. 1997; D53:240–55.
22. Bourne Y, Radic Z, Sulzenbacher G, Kim E, Taylor P, Marchot P. J. Biol. Chem. 2006; 281:29256–67. [PubMed: 16837465]
23. Emsley P, Cowtan K. Acta Crystallogr. 2004; D60:2126–32.
24. Davis IW, Leaver-Fay A, Chen VB, Block JN, Kapral GJ, Wang X, Murray LW, Arendall WB, Snoeyink J, Richardson JS, Richardson DC. Nucleic Acids Res. 2007; 35:W375–W383. [PubMed: 17452350]
25. DeLano, WL. The PyMOL Molecular Graphics System. Delano Scientific; San Carlos, CA, USA: 2002. http://www.pymol.org
26. Kuntz ID, Chen K, Sharp KA, Kollman PA. Proc. Natl. Acad. Sci. USA. 1999; 96:9997–10002. [PubMed: 10468550]

NIH-PA Author Manuscript

NIH-PA Author Manuscript

NIH-PA Author Manuscript

27. Colletier JP, Sanson B, Nachon F, Gabellieri E, Fattorusso C, Campiani G, Weik M. J. Am. Chem. Soc. 2006; 128:4526–7. [PubMed: 16594661]
28. Kryger G, Silman I, Sussman JL. Structure of acetylcholinesterase complexed with E2020 (Aricept®): implications for the design of new anti-Alzheimer drugs. Structure. 1999; 7:297–307. [PubMed: 10368299]
29. Haviv H, Wong DM, Greenblatt HM, Carlier PR, Pang Y-P, Silman I, Sussman JL. Crystal Packing Mediates Enantioselective Ligand Recognition at the Peripheral Site of Acetylcholinesterase. J. Am. Chem. Soc. 2005; 127:11029–36. [PubMed: 16076210]
30. Grochulski P, Li Y, Schrag JD, Bouthillier F, Smith P, Harrison D, Rubin B, Cygler M. J. Biol. Chem. 1993; 268:12843–7. [PubMed: 8509417]
31. Grochulski P, Li Y, Schrag JD, Cygler M. Protein Sci. 1994; 3:82–91. [PubMed: 8142901]
32. Tanaka T, Ames JB, Harvey TS, Stryer L, Ikura M. Nature. 1995; 376:444–7. [PubMed: 7630423]
33. Ames JB, Ishima R, Tanaka T, Gordon JI, Stryer L, Ikura M. Nature. 1997; 389:198–202. [PubMed: 9296500]
34. Hansen SB, Sulzenbacher G, Huxford T, Marchot P, Taylor P, Bourne Y. EMBO J. 2005; 24:3635–46. [PubMed: 16193063]
35. Hibbs RE, Sulzenbacher G, Shi J, Talley TT, Conrod S, Kem WR, Taylor P, Marchot P, Bourne Y. EMBO J. 2009; 28:3040–51. [PubMed: 19696737]
36. Gao F, Bern N, Little A, Wang HL, Hansen SB, Talley TT, Taylor P, Sine SM. J. Biol. Chem. 2003; 278:23020–6. [PubMed: 12682067]
37. Wang HL, Gao F, Bren N, Sine SM. J. Biol. Chem. 2003; 278:32284–91. [PubMed: 12799358]

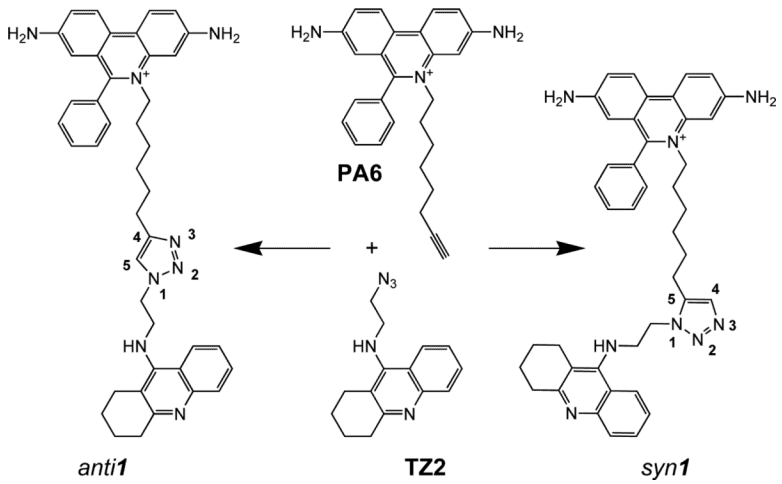

Scheme 1. Structures of the *anti1* and *syn1* TZ2PA6 regioisomers

The phenyl-phenanthridinium, triazole, and tacrine precursors and moieties are shown from top to bottom. Note the distinctive 1,2,3-triazol-4-yl versus 1,2,3-triazol-5-yl connections for the *anti1* and *syn1* isomers formed by 1,3-dipolar cycloaddition.[11]

NIH-PA Author Manuscript NIH-PA Author Manuscript NIH-PA Author Manuscript

NIH-PA Author Manuscript

NIH-PA Author Manuscript

NIH-PA Author Manuscript

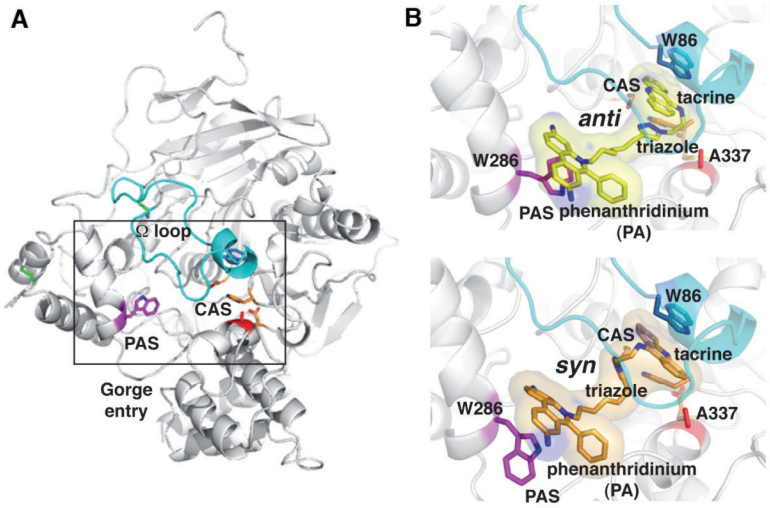

Figure 1. Overall views of the Tyr337Ala subunit and bound TZ2PA6 inhibitors

(**A**) Overall view of the mAChE-Tyr337Ala molecule (white ribbon), viewed down into the gorge. The catalytic triad residues Ser203, Glu334, His447 are displayed in orange at the center of the subunit. The long Ω loop Cys69-Cys96 is in cyan, PAS residue Trp286 is in magenta, the substituted Ala337 in red and Trp86 at the base of the gorge in blue. The three disulfide bridges respectively located in the long Ω loop, the short Ω loop (Cys257-Cys272) and between helices α(4)7,8 and α10 in the four-helix bundle are displayed as green bonds. (**B**) Close-up views of the bound *anti1* (top, yellow bonds and transparent molecular surface) and *syn1* isomers (bottom, orange bonds and surface) and surrounding side chains in the 1-mth structures (same orientation as in panel A).

NIH-PA Author Manuscript

NIH-PA Author Manuscript

NIH-PA Author Manuscript

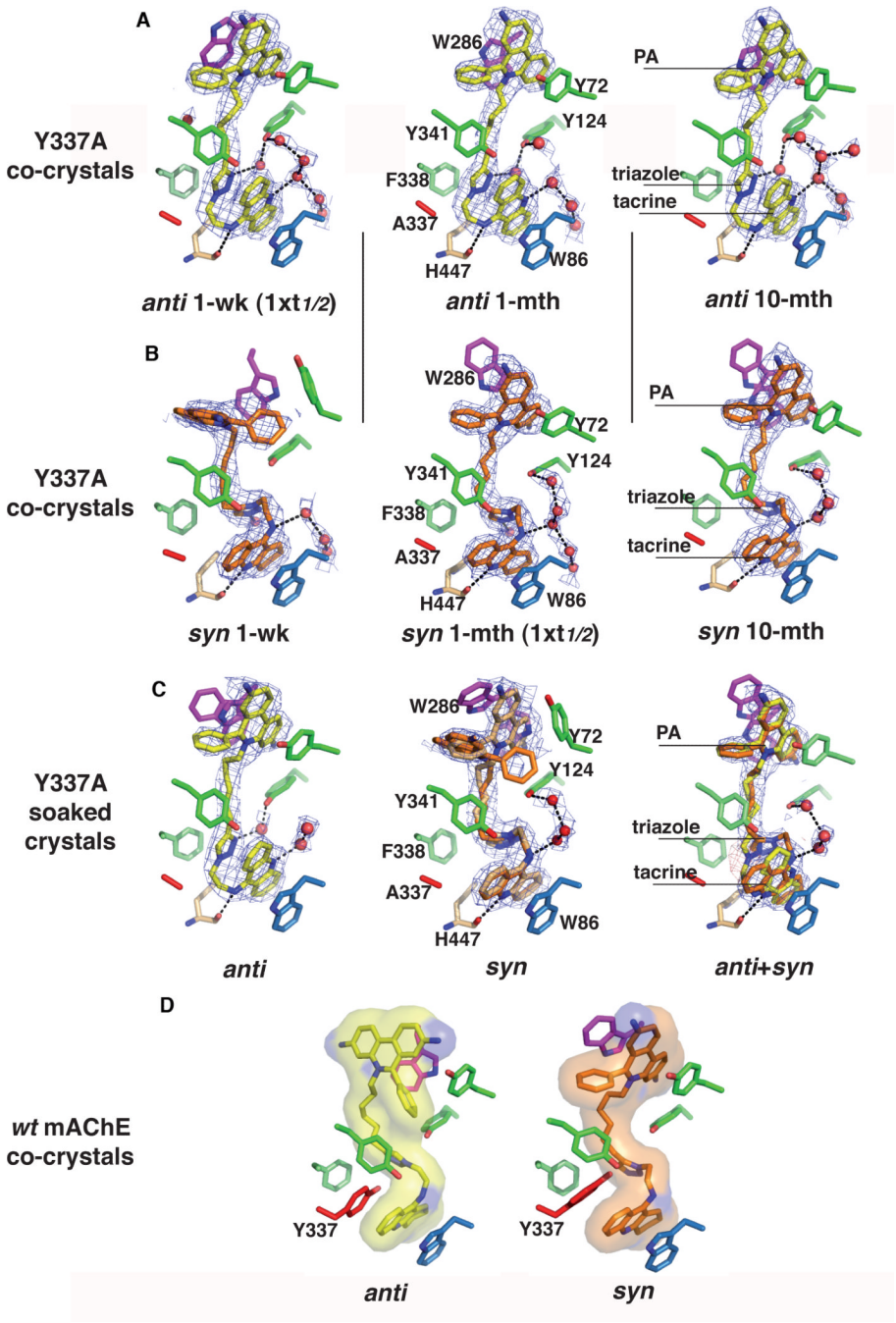

Figure 2. Close up views of the TZ2PA6-Tyr337Ala complexes

Bound *anti1* (**A**, yellow) and *syn1* (**B**, orange) in the 1-wk, 1-mth and 10-mth structures (left to right) oriented as in Fig. 1B. The respective 2.55-2.8 Å resolution final 2Fo-Fc electron density maps are contoured at 1 σ (cyan). The key interacting side chains are colored blue, green and magenta (blue nitrogens, red oxygens) for those that respectively interact with the tacrine, triazole and phenanthridinium moieties of the isomers. The catalytic His447 is displayed in light orange and the side chain of Ala337 is in red. Water molecules mediating ligand interactions are shown as red spheres. Hydrogen bonds between mAChE-Tyr337Ala, the bound isomers and the water molecules are shown as dotted lines. (**C**) Bound *anti1* (left, yellow), *syn1* (middle, orange) and *anti1*/*syn1* (right, yellow and orange, respectively) in the

structures obtained by crystal soaking. The soaked *syn1* when bound adopts two conformations. Soaking an *anti1*/*syn1* mixture leads to a predominant *syn1* and a low abundance *anti1*, as demonstrated by the positive peaks above 3.5 σ (red) in the difference density maps around the triazole moiety. (**D**) The *anti1* and *syn1* isomers as bound to mAChE (PDB codes, 1Q84 and 1Q83)[14]. The side chain of Tyr337 is shown in red. The molecular surfaces of the isomers are displayed in transparency.

NIH-PA Author Manuscript
NIH-PA Author Manuscript
NIH-PA Author Manuscript

NIH-PA Author Manuscript

NIH-PA Author Manuscript

NIH-PA Author Manuscript

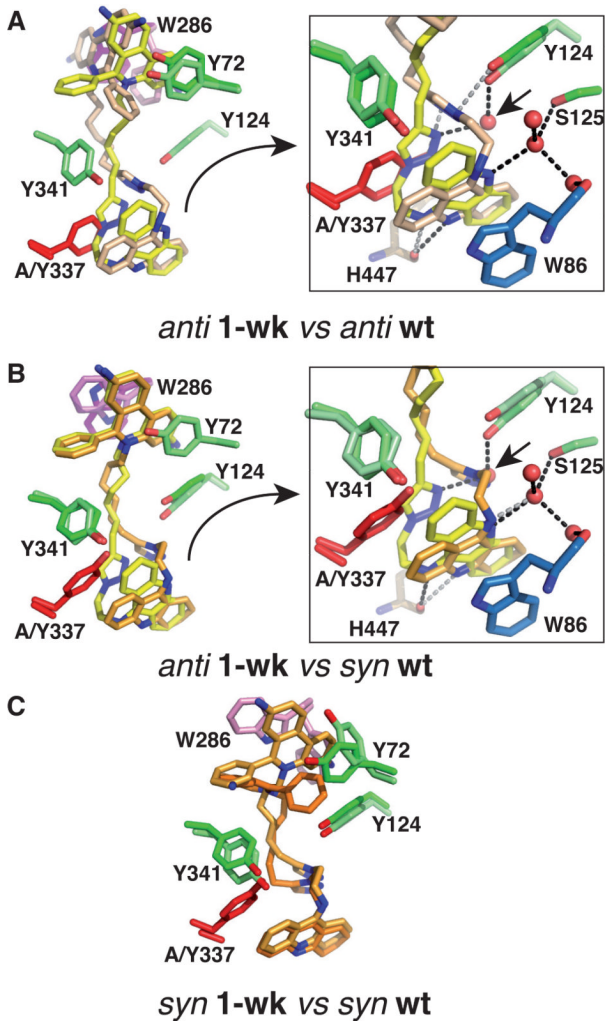

Figure 3. Comparison of the most divergent Tyr337Ala and mAChE complexes

(**A**) Overall view (left) and close up view (right) of the tacrine and triazole binding regions of overlayed *anti1* in the 1-wk structure (yellow bonds) and *anti1* bound to mAChE (light orange bonds). (**B**) Overall view (left) and close up view (right) of the tacrine and triazole binding region of superimposed *anti1* in the 1-wk structure (yellow bonds) and *syn1* bound to mAChE (light orange bonds). (**C**) Overall view of superimposed *syn1* in the 1-wk structure (orange bonds) and *syn1* in mAChE (light orange bonds). The side chains of Trp286 and of Tyr72, Tyr124 and Tyr341, which adopt distinctive positions in the complexes, are displayed in magenta/pink and in green/light green, respectively. The side chain of Ala/Tyr337 is in red and that of Trp86 in blue. The short arrow in the framed figures points to a water molecule, in the 1-wk structure of the *anti1*-Tyr337Ala complex, that mimics the triazole N2 nitrogen atom in the *syn1*-mAChE complex. Superimpositions were made according to all Cα atoms in the Tyr337Ala or mAChE subunit.

NIH-PA Author Manuscript NIH-PA Author Manuscript NIH-PA Author Manuscript

Table 1

Inhibition or binding parameters[a] for mAChE and several of its mutants and for other cholinesterases.

Enzymes and mutants	*anti1*			*syn1*		
	k_{on} (10^{10} M^{-1} min^{-1})	k_{off} (10^{-3} min^{-1})	K_d (*fM*)	k_{on} (10^{10} M^{-1} min^{-1})	k_{off} (10^{-3} min^{-1})	K_d (*fM*)
mAChE[b]	2.5	220	8900	1.7	7.1	410
mAChE mutants						
Tyr124Gln[c]	1.9	54	2800	1.2	3.9	370
Trp286Ala[b]	0.87	1800	210000	0.94	19	2000
Tyr337Ala[c]	1.6	0.066	4.1	1.3	0.013	1.0
Tyr72Asn/Tyr124Gln/Trp286Ala[c]	0.067	380	570000	0.056	77	140000
AChE, *E. electricus*[b]	1.8	250	14000	1.5	1.5	99
(conserved Tyr72, Asp74, Tyr124, Trp286, Tyr337)						
AChE, *T. californica*[b]	3.2	23	720	1.4	1.1	77
(Phe substitution for mAChE Tyr337)						
AChE, *D. melanogaster*[b]	3.4	58	1700	2.0	72	3600
(Glu, Tyr, Met substitutions for mAChE Tyr72, Asp74, Tyr124)						
Butyrylcholinesterase, mouse[b]	0.69	3.2	460	0.36	2.6	720
(Asn, Arg, Ala substitutions for mAChE Tyr72, Trp286, Tyr337)						

[a] means of n ≥ 3 individual values with SD ≤ 30% except for Tyr337Ala where SD ≤ 50%.

[b] from ref[14].

[c] this study

NIH-PA Author Manuscript NIH-PA Author Manuscript NIH-PA Author Manuscript

Table 2

Data collection and refinement statistics.

Structure	**Tyr337Ala**	**Co-crystallized complexes**						**Soaked complexes**		
Isomer		***anti1***			***syn1***			***anti1***	***syn1***	***anti1 + syn1***
Maturation time and structure name		**1-wk**	**1-mth**	**10-mth**	**1-wk**	**1-mth**	**10-mth**	**na***	**na***	**na***
Maturation vs $t_{1/2}$ for dissociation (ca.)		**1 × $t_{1/2}$**	**4 × $t_{1/2}$**	**42 × $t_{1/2}$**	**0.2 × $t_{1/2}$**	**0.8 × $t_{1/2}$**	**8 × $t_{1/2}$**	**0.15 × $t_{1/2}$**	**0.03 × $t_{1/2}$**	**na***
Data collection [a]										
Beamline (ESRF)	ID29	ID14-EH2	ID14-EH1	ID14-EH4	ID14-EH2	ID14-EH3	ID14-EH4	ID14-EH3	ID14-EH3	ID14-EH3
Wavelength (Å)	0.979	0.933	0.933	0.975	0.933	0.931	0.975	0.931	0.931	0.931
Resolution range (Å)	20 - 2.65	20 - 2.60	20 - 2.55	20 - 2.65	20 - 2.60	20 - 2.65	20 - 2.75	20 - 2.8	20 - 2.7	25 - 2.7
Total observations	204 817	235 515	255 182	233 025	228 040	222 379	204 055	256 595	276 849	273 523
Unique reflections	57 806	63 011	66 465	58 447	61 576	59 477	52 292	49 788	55 109	54 760
Multiplicity	3.5 (3.6)	3.7 (3.7)	3.8 (3.8)	4.0 (4.0)	3.7 (3.7)	3.7 (3.7)	3.9 (3.9)	5.2 (5.1)	5.0 (4.8)	5.0 (4.7)
Completeness (%)	99.1 (99.1)	100 (99.4)	99.5 (99.5)	99.7 (99.8)	98.9 (98.6)	99.0 (99.0)	99.8 (99.5)	99.8 (99.8)	99.8 (99.8)	99.7 (99.7)
I / σ (I)	12.5 (4.0)	11.8 (3.3)	15.8 (4.2)	15.4 (3.7)	13.9 (3.6)	22.4 (3.6)	15.2 (3.6)	16.6 (3.6)	17.1 (3.6)	17.3 (3.4)
Rsym[b]	7.7 (41.3)	8.8 (46.3)	5.5 (47.5)	6.5 (46.8)	5.9 (46.8)	5.4 (45.0)	7.2 (48.2)	8.9 (54.4)	8.3 (55.0)	8.4 (56.2)
B Wilson plot ($Å^2$)	57.2	61.7	58.3	68.8	66.5	65.8	71.8	72.0	65.9	68.9
Refinement [c]										
R-factor / R-free (%)	19.3 / 22.8	19.2 / 23.3	19.1 / 22.1	19.7 / 24.5	19.2 / 23.5	20.7 / 24.9	19.9 / 23.9	19.9 / 24.6	20.2 / 23.2	20.1 / 24.4
R.m.s.d. [d]										
Bonds (Å) / Angles (°)	0.012 / 1.4	0.01 / 1.49	0.01 / 1.4	0.013 / 1.5	0.012 / 1.4	0.012 / 1.5	0.01 / 1.39	0.011 / 1.58	0.01 / 1.33	0.01 / 1.33
Chiral volume ($Å^3$)	0.11	0.10	0.09	0.11	0.09	0.10	0.10	0.11	0.09	0.09
Mean B-factors (Å)										
Main chain[e]	43.0 (48.8)	49.4 (54.3)	47.6 (52.8)	52.7 (58.7)	56.0 (60.8)	53.8(59.1)	51.3 (57.9)	55.5 (61.7)	52.1 (60.0)	54.9 (60.1)
Side chain	43.9 (50.3)	50.2 (55.4)	48.7 (54.3)	53.7 (60.3)	57.4 (62.4)	54.9 (60.1)	52.1 (59.2)	56.6 (63.2)	52.9 (60.9)	55.7 (61.2)
Solvent / Carbohydrate	27.2 / -	32.5 / 80.4	30.7 / 80.6	32.7 / -	39.1 / 102.9	27.7 / -	29.7 / -	32.8 / -	27.9 / 76.7	34.5 / -
Ligand / PEG	43.5 / 42.5	55.1 / 65.0	57.3 / 91.6	60.1 / -	63.6 / 63.8	61.3 / 76.8	63.3 / -	66.9 / 65.9	50.6 / 66.1	76.0 / 71.0
PDB accession code	2XUD	2XUG	2XUF	2XUH	2XUI	2XUJ	2XUK	2XUO	2XUP	2XUQ

[a] Values in parentheses are those for the last shell.

[b] Rsym = $\Sigma_{hkl} \Sigma_i | I_{hkli} - \langle I_{hkli} \rangle | / \Sigma_{hkl} \Sigma_i \langle I_{hkli} \rangle$, where I is an individual reflection measurement and <I> is the mean intensity for symmetry-related reflections.

NIH-PA Author Manuscript

NIH-PA Author Manuscript

NIH-PA Author Manuscript

[c] R-factor = Σ ||Fo| − |Fc|| / Σ |Fo|, where Fo and Fc are observed and calculated structure factors, respectively.

[d] Root-mean-square deviation from ideal values.

[e] Values in parentheses are those for subunit B

* na, not applicable.